Water Confinement in Faujasite Cages: A Deuteron NMR Investigation in a Wide Temperature Range. 2. Spectra and Relaxation at High Temperature

ARTICLE *in* THE JOURNAL OF PHYSICAL CHEMISTRY A · JANUARY 2014

Impact Factor: 2.69

6 AUTHORS, INCLUDING:

Zdzislaw Tadeusz Lalowicz

Niewodniczanski Institute of Nuclear Physics …

79 PUBLICATIONS **538** CITATIONS

SEE PROFILE

Matthew Krzystyniak

Science and Technology Facilities Council

68 PUBLICATIONS **301** CITATIONS

SEE PROFILE

Grzegorz Stoch

Institute of Nuclear Physics

25 PUBLICATIONS **139** CITATIONS

SEE PROFILE

Kinga Góra-Marek

Jagiellonian University

73 PUBLICATIONS **509** CITATIONS

SEE PROFILE

THE JOURNAL OF PHYSICAL CHEMISTRY A

Article

pubs.acs.org/JPCA

Water Confinement in Faujasite Cages: A Deuteron NMR Investigation in a Wide Temperature Range. 2. Spectra and Relaxation at High Temperature

A. M. Szymocha,[†] Z. T. Lalowicz,*[,‡] A. Birczyński,[‡] M. Krzystyniak,[§,∥] G. Stoch,[‡] and K. Góra-Marek[⊥]

[†]University of Agriculture, 31-120 Kraków, Poland

[‡]H. Niewodniczański Institute of Nuclear Physics PAS, ul. Radzikowskiego 152, 31-342 Kraków, Poland

[§]ISIS Facility, Rutherford Appleton Laboratory, Chilton, Didcot, Oxfordshire OX11 0QX, U.K.

[∥]School of Science and Technology, The Nottingham Trent University, Clifton Lane, Nottingham NG11 8NS, U.K.

[⊥]Faculty of Chemistry, Jagellonian University, 30-060 Kraków, Poland

ABSTRACT: Deuteron NMR spectra and spin−lattice relaxation were measured for D_2O confined in NaX, NaY, and DY faujasites with various loadings at temperatures ranging from 200 to 310 K with the aim to study molecular mobility of confined water. Hysteresis of spin−lattice relaxation was observed for both DY and NaY(2.4) samples at 500% loading (280 water molecules per unit cell) in a heating−cooling cycle between 264.5 and 277.7 K. The hysteresis is most likely reflecting formation and decomposition of water clusters at different temperature. Spin−lattice relaxation rates obtained from the experiment are consistent with a picture of the fast magnetization exchange between two dynamically different deuteron populations. The observed relaxation behavior as a function of temperature and loading is most likely an effect of interplay between translational and rotational diffusion. Translational diffusion of water molecules is found to be related to the strength of the electrostatic interaction of water oxygen atoms to faujasite sodium cations, whereas water molecule reorientations seem to depend on the strength of hydrogen bonding to faujasite oxygen atoms and the strength of hydrogen bonds between water molecules, at outer and inner positions in water clusters, respectively.

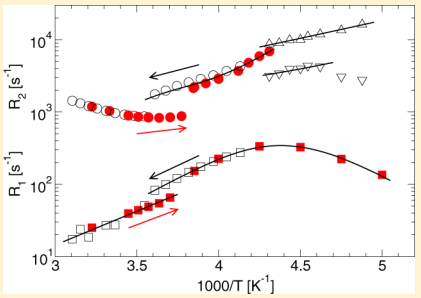

INTRODUCTION

The research on molecular confinement effects on freezing and melting has been extensively covered in review articles,[1,2] whereas the basic idea dates back to Lord Kelvin.[3] Neutron diffraction, quasielastic neutron scattering, dielectric relaxation spectroscopy, and NMR are among leading experimental methods to study molecular confinement.[4] Among many phenomena discussed in this context, the occurrence of the supercooled water phase,[5] the dynamics of the first adsorbed layer of water molecules, corroborated by molecular dynamics (MD) simulations,[6] and ice formation (as evidenced by neutron diffraction[7]) play a dominant role. Importantly for the work presented here, properties of water nanoclusters gained attention of many experimental and computational studies.[7−9] For example, water confinement in NaA zeolite was analyzed using MD simulations and the role of Na^+ cations in the formation of water clusters was emphasized.[8] Exchange between slow and fast motion sites was recently studied by NMR in D_2O confined in mesoporous MCM-41 and differences in temperature dependence of structure and mobility in slow and fast motion fractions were analyzed for different loadings.[9]

The emerging picture, based on these and other molecular probes, is that the dynamic crossover from fragile-to-strong systems of water was found to be in common for different water confining systems ranging from various zeolites, to proteins, membranes or DNA.[4] The fragile-to-strong transition (FST), predicted theoretically some time ago,[10,11] was detected by various experimental methods in a series of recent papers.[12−15] The transition temperature is clearly inferred, e.g., from the temperature dependence of the inverse of the self-diffusion coefficient. It appears as a crossover point from the non-Arrhenius to the Arrhenius behavior.[4] An underlying microscopic mechanism may be described as a transition from a state in which fully hydrogen-bonded (HB) units with some translational freedom exist, into a state characterized by long-lived clusters with internal collective jumps between HB positions in the network.[15] MD calculations indicate on FST at 225 K in computed rotational constant,[14] observed experimentally in various systems.[4]

The complex water behavior observed in many confining systems results from water bonding to the substrate and mutual interactions leading to HB clusters.[16] Interactions with some surface features in restricted geometry, electrostatic, hydrophilic, and hydrogen bonding, are of primary importance here as consecutive adsorption layers build up into various HB

Received: March 21, 2014
Revised: June 24, 2014
Published: June 24, 2014

networks, depending on the structure of the first one. It is obvious therefore to investigate adsorption as a function of loading. Moreover, measurements as a function of temperature may provide data on molecular dynamics and its symmetry, and the strength of bonding may be evaluated. Such experimental protocol is, however, restricted to substrates with temperature independent structure. Molecular dynamics simulations for argon in carbon nanopores[17] indicate that the pressure in confined structures may be very high. Experimental evidence, using neutron diffraction and DSC methods, was given for ice phases in confined water, observed otherwise in bulk samples at very high pressure.[18] Cubic clusters of water molecules were observed using X-ray diffraction in carbon fibers and in-pore pressure of the order of 4000 bar.[19]

Deuteron NMR spectroscopy and relaxation are particular suitable for studies of molecular mobility. Features characteristic for a gas phase, liquid-like layers and immobilized molecular were observed by ^{2}H NMR for some small molecules, confined in nanoscale cages of zeolites in the temperature range from 310 K down to 20 K. Translational diffusion was found to dominate in spin−lattice relaxation mechanism at high temperature, whereas features related to free rotation were observed for D_2[20] and CD_4[21] down to the low temperature range, as narrow spectra were measured in the whole temperature range. Alternatively, in the case of methanol both mutual bonding (leading to the existence of trimers) and bonding to the adsorption centers in zeolites were found to create conditions for molecular mobility.[22] Mobility of much larger organic molecules in confined space was reported, e.g., for benzene,[23] isobutyl alcohol,[24] and isobutane.[25]

This work constitutes the second paper in the sequel of NMR papers applying deuteron NMR methods to study molecular dynamics of water confined in faujasites and concentrates on the application of deuteron NMR spectroscopy and relaxometry in a wide range of temperatures. The main result of this part of our work is that narrow deuteron NMR spectra are measured down to a characteristic temperature, referred to as T_S. Below T_S spectra broadened significantly, in a stepwise manner, indicating immobilization of water molecules, as outlined in part 1.[33] Moreover, this work shows that spectral shapes, spin−lattice and spin−spin relaxation rates, as well as T_S depend significantly on Si/Al ratio and system loading with water. The picture of confined water mobility emerging from the analysis of the NMR spectra is consistent with a deuteron relaxation mechanism in which bonding to faujasite framework sodium cations and hydrogen bonding to framework oxygen atoms, as well as mutual hydrogen bonding of water molecules, plays a significant role at microscopic level. The analysis of our NMR result together with data from other experimental methods and MD simulations allows us to construct a picture of confined water mobility.

THEORETICAL PRINCIPLES: RELAXATION

The quadrupole Hamiltonian for deuteron quadrupole moment interaction with an electric field gradient (efg) can be expressed in terms of spacial Q_l and spin coordinates S_l:[26]

$$\mathcal{H}_Q^l = \frac{1}{4} h C_Q \sum_{\mu=-2}^{2} Q_1^{(\mu)} S_1^{(\mu)} \tag{1}$$

where the quadrupole coupling constant of deuterons with the electric quadrupole moment eQ, placed in an axially symmetric efg with the magnitude eq, amounts

$$C_Q = \frac{e^2 q Q}{h} \tag{2}$$

Using the perturbative approach to nuclear spin relaxation and the spin temperature approximation, we can write the initial relaxation rate of the spin system as[26]

$$R = k_1 + 2k_2 \tag{3}$$

where transition rates k_1 and k_2 are due to the time-dependent quadrupole perturbation for transitions by $\Delta m = \pm 1$ and $\Delta m = \pm 2$ between nuclear Zeeman levels, respectively.

In general

$$k_\mu = \frac{1}{h^2} |\langle 1|S^{(\mu)}|1-\mu\rangle|^2 C_Q{}^2 \int_{-\infty}^{\infty} C_R^{(\mu)}(\tau) e^{-i\mu\omega\tau}\, d\tau$$
$$\mu = 1, 2 \tag{4}$$

where $\langle 1|S^{(1)}|0\rangle = \langle 0|S^{(1)}|-1\rangle = 2^{1/2}$, $\langle 1|S^{(2)}|-1\rangle = 2$, and the correlation function

$$C_R^{(\mu)}(\tau) = \frac{1}{8} \sum_{j=1}^{n} Q_j^{(\mu)}(\tau)\, Q_j^{(-\mu)}(0)$$

depends on the details of the evolution of the deuteron position in space. For the single exponential correlation function

$$C_R(t) = \exp\left(-\frac{t}{\tau_c}\right) \tag{5}$$

commonly assumed according to the Debye model,[27,28] the spectral density function as the Fourier transform of the correlation function reads

$$j(\tau_c, \mu\omega_0) = \frac{\tau_c}{1 + \mu^2 \omega_0{}^2 \tau_c{}^2} \tag{6}$$

The relaxation rates for isotropic (multiaxial) reorientation can then be written as[26]

$$R_1 = \frac{1}{T_1} = \frac{3}{10}\pi^2 C_Q{}^2 \left(\frac{\tau_c}{1 + \omega_0{}^2 \tau_c{}^2} + \frac{4\tau_c}{1 + 4\omega_0{}^2 \tau_c{}^2}\right) \tag{7}$$

$$R_2 = \frac{1}{T_2} = \frac{3}{20}\pi^2 C_Q{}^2 \left(3\tau_c + \frac{5\tau_c}{1 + \omega_0{}^2 \tau_c{}^2} + \frac{2\tau_c}{1 + 4\omega_0{}^2 \tau_c{}^2}\right) \tag{8}$$

At high temperatures, where $\omega_0\tau_c \ll 1$, $R_1 = R_2$, whereas at temperatures below the maximum for R_1 ($\omega_0\tau_c \approx 0.616$) the relation $R_2 > R_1$ is valid. Both relaxation rates, calculated for C_Q = 260 kHz, $\tau_0 = 2.2 \times 10^{-14}$ s, E_a = 26.7 kJ/mol, are shown in Figure 1.

Water dynamics in ionic solutions was studied recently by MD simulations[29] and deuteron NMR.[30] Two processes were considered in the correlation decay: a dominating fast and a slower (diffusive) process. According to Lipari−Szabo theory developed for internal motions in macromolecules,[31,32] the total spectral density function consists of two contributions under motional narrowing conditions:[30]

$$j^{tot}(\tau_c, \mu\omega_0) = j^{fast}(\tau_c, \mu\omega_0) + j^{diff}(\tau_c, \mu\omega_0)$$
$$= \frac{a}{(1-\alpha)} \frac{\tau_c}{1 + \mu^2 \omega_0{}^2 \tau_c{}^2} \tag{9}$$

where $\alpha = j^{fast}(\tau_c, \mu\omega_0)/j^{tot}(\tau_c, \mu\omega_0)$ is approximated as frequency independent. The Lipari−Szabo constant a contains the

dx.doi.org/10.1021/jp502827x | J. Phys. Chem. A 2014, 118, 5371−5380

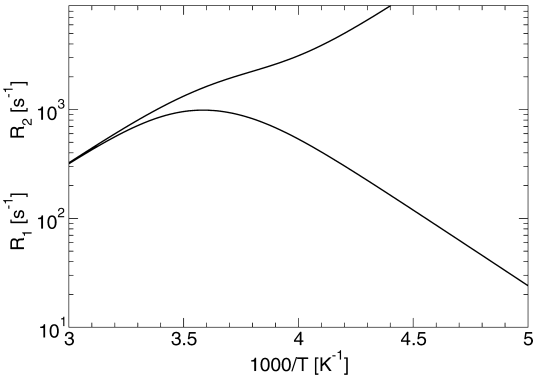

Figure 1. Temperature dependence of spin−lattice relaxation rate R_1 (eq 7) and spin−spin relaxation rate R_2 (eq 8) with a common set of parameters (see text).

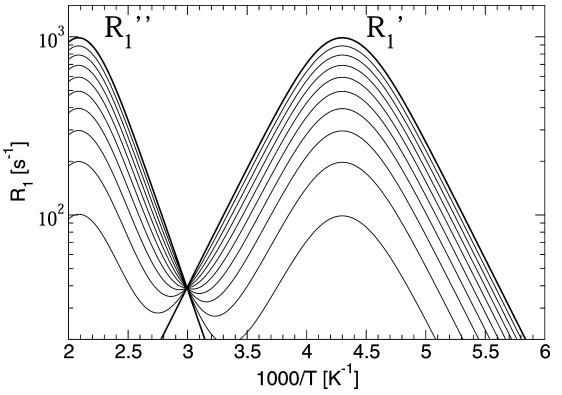

Figure 2. Deuteron spin−lattice relaxation rates R_1' and R_1'' for two subsystems under exchange (eq 11) (see text for details and parameters).

integrated contribution of the fast relaxation and the relaxation time represents the diffusive exponential tail.

Using this approximation and eqs 7 and 9 one obtains

$$R_1 = \frac{3}{10}\pi^2(C_Q^{\text{eff}})^2\left(\frac{\tau_c}{1+\omega_0{}^2\tau_c{}^2} + \frac{4\tau_c}{1+4\omega_0{}^2\tau_c{}^2}\right) \tag{10}$$

where $C_Q^{\text{eff}} = A^{1/2}C_Q$ and $A = a/(1-\alpha)$. The above approximation is directly applicable to our experimental results, which provide an effective quadrupole coupling constant C_Q^{eff}, which is significantly smaller than C_Q measured for motionless molecules.

In the following a spin system will be assumed to consist of two subsystems characterized by a fast and slow motional regime with intrinsic relaxation rates R_1' and R_1'', respectively. In the limit of the fast magnetization exchange between the subsystems a single apparent relaxation rate can be observed:

$$R_1 = WR_1' + (1-W)R_1'' \tag{11}$$

where W depends on relative abundances of molecules in both subsystems and R_1' and R_1'' are expressed by eq 7, however, for different correlation times. Experimentally, the limit of the applicability of eq 11 is described by the temperature T_S. Above T_S narrow deuteron NMR lines are observed. Below T_S a substantial, stepwise broadening of deuteron spectra appears, and magnetization recovery becomes nonexponential.[33]

Figure 2 shows the simulation of the relaxation rate R_1, expressed by eq 11, as a function of inverse temperature $1000/T$ in the range 3.3 K^{-1} < $1000/T$ < 4.5 K^{-1}, relevant for the experimental results shown, for values of the parameter W changing from 0 to 1 in 0.1 steps. The relaxation rate R_1' was calculated assuming $C_Q' = 260$ kHz, $\tau_0' = 4 \times 10^{-15}$ s, $E_a' = 25.5$ kJ/mol, whereas for R_1'' $C_Q'' = 260$ kHz, $\tau_0'' = 2.0 \times 10^{-13}$s, $E_a'' = 37.0$ kJ/mol were assumed.

Seeing that the fast two-site deuteron exchange produces an exponentially decaying longitudinal magnetization curve in time domain we proceed to the description of the transversal deuteron spin relaxation for confined heavy water molecules. For a cluster of heavy water molecules exhibiting local tetrahedral symmetry and exchanging rapidly within a set of orientations related by tetrahedral symmetry a very narrow ^{2}H NMR line is observed, as the quadrupole spin Hamiltonian averages to zero analytically.

In liquids, where Brownian motion dominates, the shape of the NMR line has the form of Lorentzian distribution. A local potential of a water molecule in a cluster is fluctuating in time and space due to oscillating distance between neighboring molecules as well as due to their rotation. Under favorable conditions consecutive rotations may take place between tetrahedrally related temporary positions of some water molecules whereas other molecules may perform less specified isotropic reorientation. In such a picture we may expect two narrow spectral components with different widths and relative contributions being temperature dependent.

The transverse magnetization observed after a 90° pulse, is given by[34,35]

$$\langle M_+(t)\rangle = iM_0 \exp(-i\omega_0 t)\cos(\omega' t) \tag{12}$$

For confined water molecules one may consider a local, molecular reference frame (x', y', z') with the z' axis along the 2-fold symmetry axis with position defined by polar and azimuthal angles θ' and ϕ' in the laboratory reference frame. The orientation of a water deuteron in the molecular reference frame is characterized by angles θ'' and ϕ''. With this parametrization, motional average of the quadrupole shifts can be written as[34,36]

$$\omega' = \frac{3}{16}C_Q(3\cos^2\theta' - 1)\langle 3\cos^2\theta'' - 1\rangle_{\text{av}} \tag{13}$$

For a spin system consisting of localized, differently oriented water molecules experiencing different mobility a Gaussian distribution of ω' values is expected, with the mean value ω_0:

$$G(\Delta\omega') = \exp\left(\frac{-\Delta\omega'^2}{2\sigma^2}\right) \tag{14}$$

where $\Delta\omega' = \omega' - \omega_0$ and σ is the width of the distribution. The average of the cosine term in eq 12 is given by

$$\langle\cos(\omega' t)\rangle_{\text{av}} = \cos(\omega_0 t)\int_{-\infty}^{+\infty}\cos(\Delta\omega' t)\,G(\Delta\omega')\,d(\Delta\omega') \tag{15}$$

which yields

$$\langle\cos(\omega' t)\rangle_{\text{av}} = \cos(\omega_{\text{av}}' t)\exp\left(\frac{-\sigma^2 t^2}{2}\right) \tag{16}$$

Most importantly, in the case of our experimental NMR data on confined water no oscillations were detected in the free induction decay signal (FID), thus leading to featureless spectra. This experimental observation corresponds to the

dx.doi.org/10.1021/jp502827x | J. Phys. Chem. A 2014, 118, 5371−5380

condition $\omega'_{av} = 0$. In such case, the magnetization in the rotating reference frame along the y-detection axis is given by

$$M_y(t) = M_L \exp\left(-\frac{t}{T_2}\right) + M_G \exp\left(-\frac{\sigma^2 t^2}{2}\right) \quad (17)$$

Defining T_2 as the time constant corresponding to the magnetization decay by the factor $1/e$ compared to its initial value, from the second term in eq 17 we get $T_2 = 2^{1/2}/\sigma$. Fourier transform relates T_2 and the full-width at half-maximum of the spectral line, h (FWHA), leading to the relations $h = 2/T_2$ and $h = [2(\ln 2)^{1/2}]/T_2$, for the Lorentzian and Gaussian line shapes representing liquid-like water molecules with translational and rotational freedom and water molecules restricted in their fast reorientations, respectively.

EXPERIMENTAL RESULTS AND DISCUSSION

Experimental setup and sample preparation had been described in part 1.[33] The loading level is defined also here with respect to the abundance of sodium cations in the respective unit cell. The ratio Si/Al defines the composition of a faujasite, which is $Na_{86}[(SiO_2)_{106}(AlO_2)_{86}]$ for NaX(1.3). Thus, the abundance of sodium cations is related to the Si/Al ratio, the value of which is given in brackets following the name of the faujasite.

NMR spectra were obtained by the Fourier transformation of the free induction decay (FID). For eliminating spectral baseline distortion, an extension[37] of Heuers method[38] dedicated to wide spectra was used. The nature of quadrupole interaction for deuterons allows us to expect symmetric spectra. Thus, the zeroing of the imaginary signal was possible at the final stage of signal processing. An acceptable signal-to-noise ratio in the spectra was achieved by signal averaging over several thousands of accumulations depending on loading. Repetition time was kept at least 5 times longer than the time constant observed in relaxation.

Spectra. When dealing with the phenomenon of geometrical confinement of small molecules, an NMR experimentalist is equipped with a whole arsenal of nuclear spin observables, among which, apart from the spectral shape characteristics, spin−spin and spin−lattice relaxation time constants seem to be an obvious choice in the case of site-specific quadrupole spin probes like the deuteron. In the following we start the extensive characterization of water confined in faujasites by describing the results of the analysis of deuteron spectra at a wide range of temperatures. The Lorentzian line shape appears at higher temperatures indicating a high translational mobility. The Gaussian spectral components, with a width related to differences in efficiency of almost isotropic reorientation, refer to localized molecules. The main spectral NMR observables are in this case spectral widths and, in the case of structured spectral lines, numbers of different spectral components with distinct shapes and their relative contributions.

Concretely, in the case of the spectra measured in DY zeolite with 500% loading, a transition is observed from Lorentzian shape at about 232.5 K into two superimposed Gaussian components. Examples of spectra obtained at 250 and 222.5 K are shown in Figure 3. The Lorentzian component broadens above 263 K, as expected for a thermally activated process, and the analysis of the thermal broadening leads to the estimate for the activation energy, E_a = 23.1 kJ/mol. Such temperature dependence is also observed in the case of Gaussian spectral components, leading to activation energies of E_a = 8.7 kJ/mol

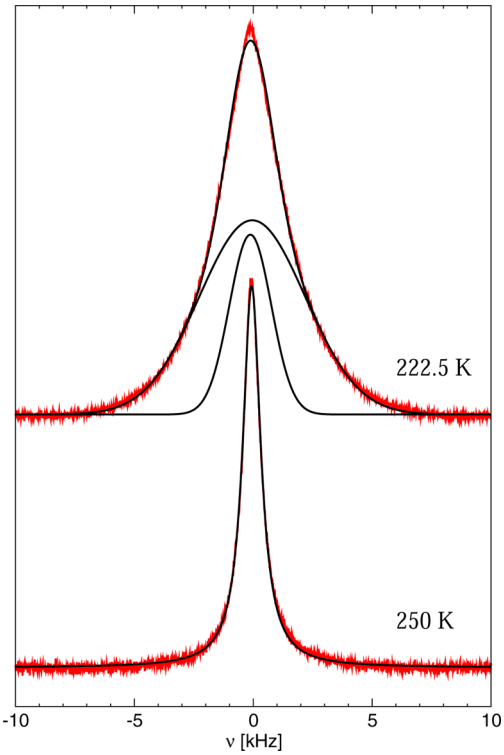

Figure 3. Examples of deuteron spectra for DY zeolite with 500% loading of D_2O.

and E_a = 9.2 kJ/mol for the narrow and the broad Gaussian component, respectively (Figure 4). The shape of the

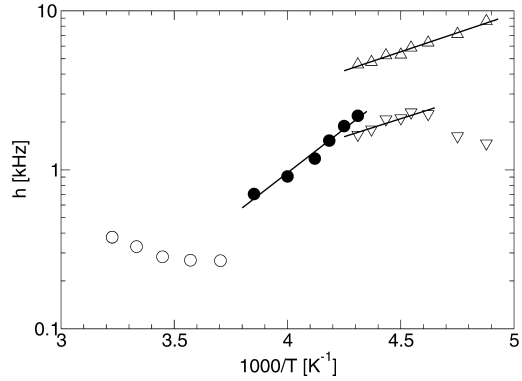

Figure 4. DY sample with 500% loading of D_2O. Temperature dependence of spectral width h (FWHA) for Lorentzian (○, ●), narrow (▽), and broad (Δ) Gaussian line shapes. Linear fits lead to the estimation of the activation energies listed in Table 1.

Lorentzian component shows no temperature dependence above 263 K, within the limits of instrumental resolution due to the magnetic field inhomogeneity (0.1 kHz), and is constant with the width of about 0.3 kHz. The contribution of the narrow Gaussian spectral component is decreasing (corresponding to the activation energy of E_a = 37.1 kJ/mol) and the contribution of broad Gaussian component increases (corresponding to E_a = 7.6 kJ/mol). Activation energies obtained from spectral line-widths and contributions of Gaussian spectral components are listed in Table 1, where values obtained above and below T_{50} are marked HT and LT, respectively.

dx.doi.org/10.1021/jp502827x | J. Phys. Chem. A 2014, 118, 5371−5380

Table 1. Temperature T_{50} and Activation Energies E_a Derived for Contributions and Line Width of the Gaussian Spectra

		E_a [kJ/mol]							
		contributions				line width			
		narrow line		broad line		narrow line		broad line	
sample, loading	T_{50} [K]	HT	LT	HT	LT	HT	LT	HT	LT
NaX(1.3), 100%	245.0	4.0	20.9	7.1	7.1	28.3	28.3	24.4	24.4
NaY(1.8), 100%	311.0	10.2	10.2	4.9	4.9	16.9	16.9	17.1	17.1
NaY(2.4), 100%	305.0	11.1	11.1	4.9	4.9	10.0	10.0	11.0	11.0
DY, 100%	245.0		23.3		7.7		16.0		8.5
NaX(1.3), 300%	305.0	11.4	11.4	4.8	4.8	15.7		14.8	
NaY(1.8), 300%	260.0	4.0	58.4	3.8	14.9	17.0	17.0	17.4	17.4
NaY(2.4), 300%	235.0	4.8	53.4	3.5	12.4	11.9	33.1	13.0	27.8
NaX(1.3), 500%	294.0	11.2	11.2	5.6	5.6	15.2	15.2	13.5	13.5
NaY(2.4), 500%	250.0	5.4	5.4	6.4	6.4	6.3	46.7	7.0	42.5
DY(2.4), 500%	240.0		37.1		7.6	21.1	8.7		9.2

Results for DY with 100% loading are similar to the case of 500% loading with the transition from a narrow to a broad Lorentzian spectral component observed at 274 K and the transition into two Gaussian components at 241 K.

The Lorentzian component is absent in NaY(2.4) zeolite with 500% loading. Two Gaussian components are observed starting from the highest temperature. At about 263 K both Gaussian components broaden significantly and activation energies increase by an order of magnitude (Table 1). A similar transition was observed for NaY(2.4) with 300% loading at 244 K, however, with a less dramatic change in activation energies (Figure 5). Activation energies of the narrow and the broad Gaussian component are very similar in the whole range of temperatures, and there is no transition in the width as a function of temperature for NaY(2.4) with 100% loading. A continuous broadening of the Gaussian component is, however, observed for NaX(1.3) with 500% and 300% loading. Concretely, in the case of NaX (1.3) with 100% loading a transition in Gaussian component width is observed. Moreover, at 277 K an abrupt decrease of the narrow Gaussian component contribution is observed below 250 K, corresponding to a significantly higher activation energy.

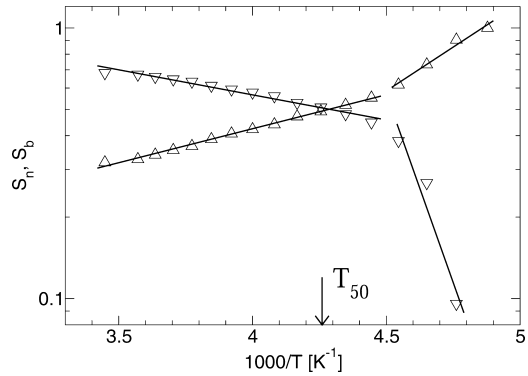

Figure 5. NaY(2.4) sample with 300% loading of D_2O. Temperature dependence of relative contributions S_n and S_b, of the narrow (▽) and the broad (Δ) Gaussian spectral components, respectively. Linear fits lead to the estimation of the activation energies listed in Table 1.

Analysis of the temperature dependence of relative contributions of Gaussian spectral components provides more information on the mobility of water molecules as a function of Si/Al ratio in faujasite and the faujasite loading. Difference in the width of Gaussian components is related to the efficiency of nearly isotropic reorientation in averaging intramolecular spin interactions. At T_{50}, contributions of both Gaussian components are equal, whereas above T_{50} the contribution of the narrow component prevails. Therefore, we choose T_{50} as a significant parameter, indicating differences in the molecular mobility. The contribution of the narrow Gaussian component reaches zero for temperatures approaching T_S.

Temperature T_{50} increases with increasing Si/Al ratio for samples with 100% loading. The contribution of the narrower Gaussian component at 310 K amounts to about 73% and about 56% for NaX and NaY, respectively. As indicated before, the interaction of water oxygen with sodium cation in NaY is stronger than in NaX. This explains higher T_{50} and lower abundance of more mobile molecules in NaY. The data for loadings 300% and 500% indicate a reversed dependence on Si/Al ratio (Table 1). Molecules in cages outnumber positions at sodium cations. Translational mobility combined with formation of clusters introduce more possibilities in interactions with the framework. As mentioned above, hydrogen bonding of water deuterons with framework oxygen atoms is weakest in the zeolite NaY resulting in the number of more mobile water molecules being higher at high temperature. Narrow Gaussian contribution amounts to about 73% in NaY and about 44% in NaX at 294 K at 300% loading. A similar relation occurs for 500% loading. Some more conclusions can be drawn when the dependence of activation energy on Si/Al ratio at constant loading is considered (Table 1).

The characterization of dynamically different deuteron spin subsystems for heavy water confined in zeolites, from the analysis of the temperature behavior of ^2H NMR spectral components, can be further detailed by comparing the effects of spin−spin and spin−lattice relaxation, which is the subject of the following section.

Relaxation. The relaxation measurements are based on recording signal amplitudes on time after $\pi/2$ pulse leading to the magnetization recovery $M(t)$. The amplitudes were quantified by FID signal integration beyond the receiver dead time. The spin−lattice relaxation rate was derived by fitting the magnetization recovery with $M(t) = M_\infty[1 - \exp(-t/T_1)]$. A sequence of measurements at different temperatures within a chosen range provides the temperature dependence of the relaxation rate.

The temperature dependence of the spin−lattice relaxation R_1 was fitted to experimental results for all samples listed in

dx.doi.org/10.1021/jp502827x | J. Phys. Chem. A 2014, 118, 5371−5380

Table 2. Parameters Obtained from Relaxation Data (E_a, kJ/mol)

	spin−lattice, R_1				spin−spin, R_2					
						E_a(Gn)[a]		E_a(Gb)[b]		
sample, loading	E_a	C_Q^{eff} [kHz]	A	W	E_a(L)	HT	LT	HT	LT	T_S [K]
NaX(1.3), 100%	18.6	143.3	0.30	0.30			42.5		27.5	220.0
NaY(1.8), 100%										235.0
NaY(2.4), 100%	9.8	87.8	0.11	0.13		18.0	18.0	12.1	12.1	225.0
DY, 100%	23.0 LT	148.6	0.33	0.34	27.1		21.5		8.5	200.0
	9.8 HT									
NaX(1.3), 300%	11.4	136.1	0.27	0.22		27.0	27.0	15.0	15. 0	233.0
NaY(1.8), 300%	14.3	139.4	0.29	0.30		17.9	28.8	30.9	13.7	210.0
NaY(2.4), 300%	23.3	149.4	0.33	0.35		13.4	53.0	19	28.5	205.0
NaX(1.3), 500%	11.0	133.0	0.26	0.25		21.5	21.5	12.7	12.7	227.0
NaY(2.4), 500%	31.7 LT	153.7	0.35	0.35		6.8	68.9	7.6	34.5	218.0
	36.5 HT	98.6	0.14	0.11						
DY(2.4), 500%	23.7 LT	153.3	0.35	0.35	26.6		10.7		9.7	205.0
	18.0 HT	180.0	0.48	0.48						

[a] E_a(Gn) - activation energy for narrower Gaussian [b] E_a(Gb) - activation energy for broader Gaussian.

Table 1, using the model described in eq 7. Fitting the model to the relaxation data yielded in all cases activation energies and values of the effective coupling constant C_Q^{eff} < 260 kHz with corresponding values of $A = (C_Q^{eff}/C_Q)^2$ (Table 2). Alternatively, fitting the results of the spin-relaxation rate R_1' (eq 11) we obtained comparable values of the parameter W (Table 2).

Values of the spin−spin relaxation rate were obtained from the width of the recorded spectra, $R_2^L = h/2$ and $R_2^G = h/[2(\ln 2)^{1/2}]$ of Lorentzian and Gaussian spectral components, respectively. The relaxation rates were fitted with eq 8 and activation energies listed in Table 2. Relation $R_2 > R_1$ holds in all cases and in the whole temperature range, which makes an interpretation unambiguous for all figures showing both relaxation rates.

Interestingly, hysteresis was observed in the temperature dependence of both R_1 and R_2 for DY sample with 500% loading (Figure 6). A stepwise increase was observed in R_2 at 263 K and a transition into a lower relaxation rate R_2 at 277.8 K, on cooling and heating the system, respectively. Fitting R_2 with eq 8 in the range from 277.8 K down to 232.5 K provides an upper conservative bound for the effective coupling constant, C_Q = 260 kHz with E_a = 26.7 kJ/mol and $\tau_0 = 2.2 \times 10^{-14}$ s. Similar results would be obtained for such a phase of confined water existing in the whole temperature range. Temperature dependence of R_1 and R_2, calculated with these values of the parameters, is shown in Figure 1. However, the temperature dependence of R_2 from 322 K down to 263 K cannot be described using eq 8. Thus, no correlation time can be assigned from the temperature dependence of R_2 according to the Arrhenius formula.

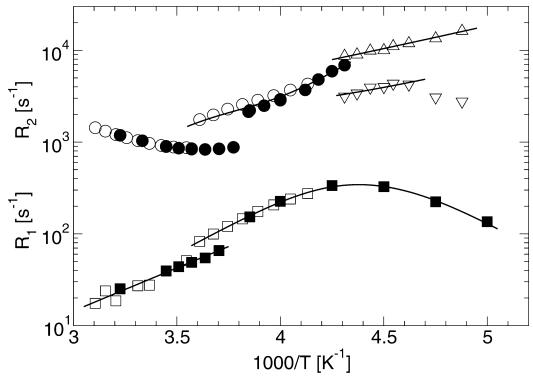

Figure 6. Temperature dependence of deuteron relaxation rates R_1 and R_2 for DY sample with 500% loading of D_2O. Symbols ○, ● and □, ■ refer to spin−spin R_2 and spin−lattice R_1 relaxation rates, respectively. Filled and open symbols represent results obtained on cooling and heating, respectively. Narrow and broad Gaussian components are denoted with (▽) and (Δ) symbols, respectively.

Below 232 K there are two distinct R_2 relaxation rate constants, related to two separate Gaussian components (Figure 6). Correlation times, τ_c, obtained at the transition temperature 232.5 K are almost equal and read 2.2×10^{-8} s for the Lorentzian component, and 2.7×10^{-8} and 1.7×10^{-8} s for the Gaussian components, respectively. Such a result would indicate that the transition observed in relaxation is not related to rotational diffusion, but rather to a significant reduction of translational diffusion, most likely related to the fragile-to-strong crossover transition.[4] At the molecular level, the transition may be described as development of a network of strongly HB molecules from a set of local weakly HB networks.[12] The maximum of the spin−lattice relaxation rate R_1 appears in the same range of temperatures. The position of the maximum provides, via condition $\omega_0\tau_c \approx 0.616$, the value of the correlation time, $\tau_c = 2.1 \times 10^{-9}$ s. The effective correlation time deduced from the relaxation rate R_1 is 1 order of magnitude shorter than that from R_2, as it results from a contribution of exchange jumps. The hysteresis was observed also for the R_1 relaxation rate (Figure 6). There is a stepwise increase at 263.2 K on cooling, and a slowing down at 277.8 K on heating. Fitting with eq 7 provides parameters in Table 2, for high (HT) and low (LT) temperature range, respectively.

For the DY sample with 100% loading no hysteresis was observed, as there are not enough water molecules available for construction of clusters (Figure 7). The transition from non-Arrhenius to Arrhenius behavior in spin−spin relaxation takes place at about 274 K. At this point there is also a stepwise change in the spin−lattice relaxation rate, at higher temperature than observed for DY with 500% loading. At the microscopic level it means that translational diffusion is significantly reduced in the first adsorption layer.

An unusual temperature dependence of the spin−lattice relaxation rate was observed before for D_2,[20] CD_4,[21] and

dx.doi.org/10.1021/jp502827x | J. Phys. Chem. A 2014, 118, 5371−5380

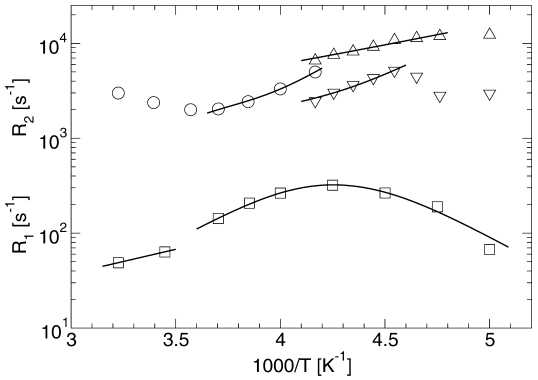

Figure 7. Temperature dependence of deuteron relaxation rates R_1 and R_2 for DY sample with 100% loading of D_2O.

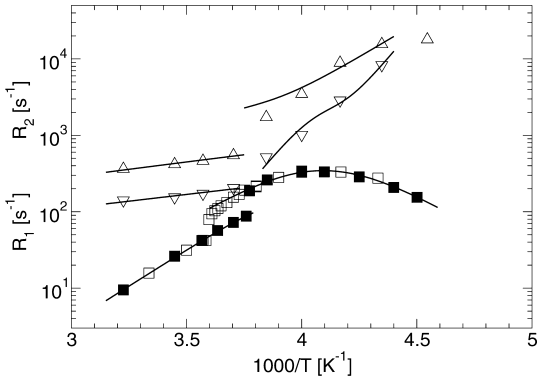

Figure 8. Temperature dependence of deuteron relaxation rates R_1 and R_2 for NaY(2.4) sample with 500% loading of D_2O. Filled and open symbols represent results obtained on cooling and heating, respectively.

CD_3OD[22] confined in zeolite cages. Two distinct relaxation mechanisms above and below the transition temperature at ca. 250 K, corresponding to two different motional regimes of the host molecules inside cages, were identified from the analysis of the relaxation data. In this picture, intramolecular spin interaction is perturbed via molecular collisions and collisions of molecules with zeolite cage walls above the transition temperature. where diffusion dominates. Many such collisions are necessary to drive spin−lattice relaxation and the effective correlation time is long. Consequently, rotation of molecules provides an efficient spin−lattice relaxation mechanism below the transition temperature, a situation commonly referred to as the weak collision case, as evidenced by previous ^2H NMR relaxation work on D_2 and CD_4 confined in zeolites.[20,21]

The effect of the transition from translation to reorientation, described above, may also be present in the case of confined water in zeolites. In this case, however, the picture is even more complicated, due to the fact that water molecules may be adsorbed on zeolite cage walls and form HB clusters. In this case bonding reduces translational mobility of water deuterons and the effective mechanism driving the deuteron spin relaxation is related more to breaking of hydrogen bonds mediated by translation. Consequently, there is no correlation between a spin state before and after a bond breaking event, which results in a drastic change in magnitude the quadrupole coupling. In such a situation another mechanism may become effective, referred to as a strong collision case, manifested by the observation of Lorentzian spectra at high temperature.[26] Taking into account all mechanisms described above, the following physical picture emerges that is most likely to describe the molecular motion responsible for water-induced nuclear spin relaxation in zeolites. At low temperatures, stable smaller water clusters may reorient as a whole in zeolite cages. However, growing clusters may render rotational diffusion ineffective. Thus, the hysteresis observed in relaxation rate constants may be attributed to a process of a local decomposition of clusters at a temperature that is higher than the temperature required for the cluster formation.

Relaxation rate constants, R_1 and R_2, measured for NaY(2.4) with 500% loading are shown in Figure 8. Hysteresis was observed in R_1 between 277.7 and 264.5 K. R_1 values measured up to 264.5 K were fitted with eq 7 with C_Q^{eff} = 98.6 kHz, E_a = 36.5 kJ/mol, and $\tau_0 = 4.7 \times 10^{-17}$ s, whereas the maximum was fitted with C_Q^{eff} = 153.7 kHz, E_a = 31.6 kJ/mol, and $\tau_0 = 3.6 \times 10^{-16}$ s. Though hysteresis in R_1 appears very similar to the case described above for DY sample with the same loading (Figure 6), there are substantial differences in observed spectra. Instead of a single Lorentzian component, two Gaussian components were observed at high temperature. Two relaxation rate constants R_2, corresponding to Gaussian components, were observed in the whole temperature range above T_S. Most interestingly, however, there is a dramatic change in the values of activation energies describing the temperature dependence of the rate constants R_2 at about 264.5 K (Table 2), but the correlation times obtained from the temperature dependence of R_1 and R_2 are very similar in the whole temperature range up to 264.5 K. The emerging physical picture that may account for this temperature behavior of relaxation rate constants is the following. The presence of sodium cations in the zeolite reduces translational mobility as the sodium−water interaction immobilizes water molecules and stimulates water cluster formation. The transition due to formation of localized water clusters appears at the same temperature as for DY sample but, in spite of the same loading, internal mobility within the clusters is strongly reduced as activation energies are much higher, being comparable to those derived from R_1. Outer molecules in the clusters may exhibit high degree of rotational mobility. Their number is highly reduced due to bonding to sodium cations leading to very different activation energies in NaY zeolites, as compared to their DY counterparts.

Characteristic temperatures of hysteresis in the spin−lattice relaxation are practically the same for DY and NaY samples with 500% loading of D_2O, which excludes the possibility of sodium cations playing an active role in this phenomenon. Such conclusion is further corroborated by considering experimental results for NaX sample with 500% loading. There are no transitions in observed relaxation rates (Figure 9) and thus no related stepwise changes in molecular mobility. The structures of all faujasites are identical. However, the loading, related to the number of sodium cations, is 50% higher in NaX than in NaY. Thus, the number of water molecules in the unit cell is consequently higher. Higher density limits diffusion and stable clusters exist in the whole temperature range above T_S. Hydrogen bonding of water deuterons with framework oxygen atoms influences the stability of clusters in NaX. The framework oxygen atoms in the zeolite NaX are more negative than in NaY. Consequently, the hydrogen bond is stronger and external water molecules in the clusters are less mobile. As mentioned above, the relative contribution of narrow Gaussian spectral component is related to the abundance of more mobile water molecules. That contribution at 294 K amounts to 70%

dx.doi.org/10.1021/jp502827x | J. Phys. Chem. A 2014, 118, 5371−5380

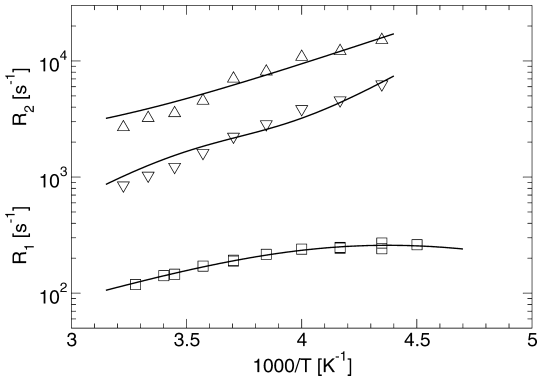

Figure 9. Temperature dependence of deuteron relaxation rates R_1 and R_2 for NaX(1.3) sample with 500% loading of D_2O.

for NaY and 55% for NaX, both at 500% loading, respectively. The reduced number of mobile molecules at outer positions in water clusters confirms relatively stronger bonding to the framework oxygen atoms in NaX. Moreover, also the activation energy, derived from the temperature dependence of narrow Gaussian component contribution, is much higher for the case of NaX (Table 1).

There is no hysteresis observed in R_1 for NaY(2.4) sample with 300% loading (Figure 10). There are 258 molecules per

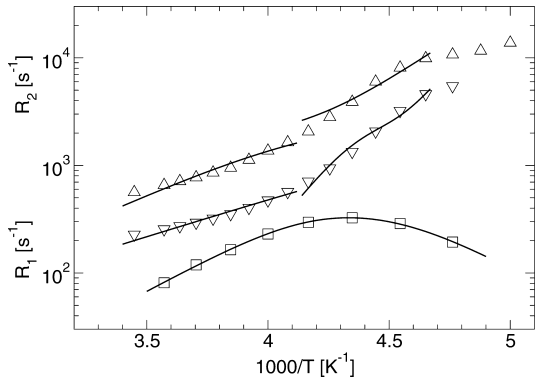

Figure 10. Relaxation rate constants R_1 and R_2 for NaY(2.4) sample with 300% loading of D_2O.

unit cell for NaX sample with 300% loading, close to 280 molecules in NaY with 500% loading. Thus, the densities of the molecules are quite similar. However, no hysteresis in R_1 is observed. The temperature dependence of R_2 is similar to that observed for the case of 500% loading; however, the transition appears now at 242 K. The temperature dependence of R_1 and R_2 for NaX(1.3) and NaY(1.8) samples with 300% loading is similar to that in the case of the NaY(2.4) sample (Figure 10, Table 2). The results of the relaxation measurements for NaX(1.3) and NaY(2.4) samples with 100% loading are shown in Figures 11 and 12, respectively. The transition in R_2 appears at 274 K in NaX(1.3). All activation energies derived for the NaX sample are higher than for the NaY case (Table 2). These observations can be reconciled within the following picture. Much stronger hydrogen bonding to framework oxygen atoms on the cage walls in NaX restricts the mobility of outer molecules in clusters that remain stable up to relatively high temperatures. Water molecules in NaY with 100% loading are more strongly localized at places where sodium cations are located. However, their reorientations are hindered by weaker

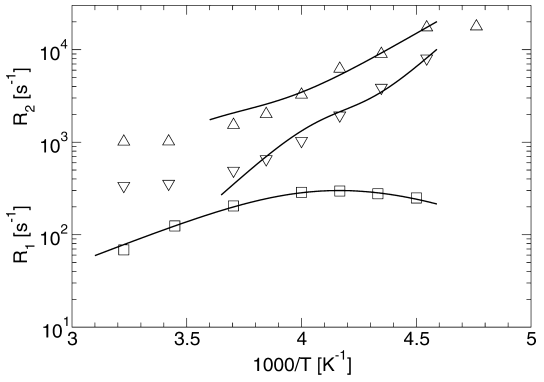

Figure 11. Relaxation rate constants R_1 and R_2 for NaX(1.3) sample with 100% loading of D_2O.

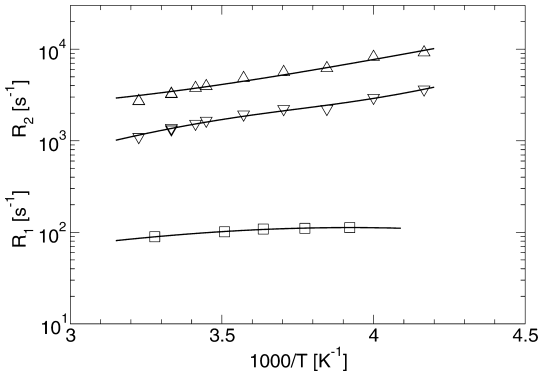

Figure 12. Temperature dependence of deuteron relaxation rates R_1 and R_2 for NaY(2.4) sample with 100% loading of D_2O.

interactions with surrounding oxygen atoms (Table 2). Alternatively, in the case of NaX(1.3), in spite of the higher abundance of more mobile water molecules at high temperature due to the weaker bonding to sodium cations, the hydrogen bonding to framework oxygen atoms hinders the reorientation.

CONCLUSION

Extensive deuteron NMR work on confined water in nanoscale faujasite cages is presented. The work advocates a coherent approach to the characterization of heavy water dynamical and binding properties in confined geometry of this mineral group in the zeolite family of silicate minerals employing a simultaneous measurement of deuteron spectra and relaxation in a wide range of temperatures for samples with selected Si/Al ratio and for different loadings. For each faujasite under investigation a set of activation energies and quadrupole coupling constants is derived from the analysis of the relaxation data. The analysis leads to the identification of two characteristic temperatures, T_S and T_{50}. The former temperature, T_S, is defined as the temperature at which instantaneous broadening of deuteron spectra occurs. The latter temperature, T_{50}, is defined as the temperature at which contributions of both Gaussian spectral components are equal. Above T_{50} the contribution of the narrow Gaussian component prevails.

The advocated approach is shown to lead to two important results. First, it provides evidence for a new phenomenon, namely a hysteresis in relaxation rates observed for DY and NaY samples with 500% loading. Second, owing to the difference in sensitivity of rotational and translational correlation times to temperature changes, the adopted

dx.doi.org/10.1021/jp502827x | J. Phys. Chem. A 2014, 118, 5371−5380

approach allows us to discriminate between competing molecular interactions driving nuclear spin relaxation of confined molecules and to identify dynamically different populations of confined molecules. Following the application of NMR-based methods demonstrated in this work, further work is clearly required to characterize water confinement and molecular dynamics in faujasites at microscopic level, which requires MD and DFT simulations.

AUTHOR INFORMATION

Corresponding Author

*Z. T. Lalowicz. E-mail: Zdzislaw.Lalowicz@ifj.edu.pl. Phone: +48 12 6628259. Fax: +48 12 6628458.

Notes

The authors declare no competing financial interest.

ACKNOWLEDGMENTS

Preliminary results, obtained during 2006−2009, were funded under Research Grant No. 202 08931/0621 by the Ministry of Science and Higher Education, Poland. Subsequent work was funded under Grant No. N202 12 17939 from the National Science Center, Poland during 2010-2014.

REFERENCES

(1) Christenson, H. K. Confinement Effects on Freezing and Melting. *J. Phys.: Condens. Matter* **2001**, *13*, R95−R133.

(2) Alba-Simionesco, C.; Coasne, B.; Dosseh, G.; Dudziak, G.; Gubbins, K. E.; Radhakrishnan, R.; Śliwińska-Bartkowiak, M. Effects of Confinement on Freezing and Melting. *J. Phys.: Condens. Matter* **2006**, *18*, R15−R68.

(3) Thomson, W. On the Equilibrium of Vapour at a Curved Surface of Liquid. *Philos. Mag. IV* **1871**, *42*, 448−452.

(4) Mallamace, F.; Corsaro, C.; Baglioni, P.; Fratini, E.; Chen, S.-H. The Dynamical Crossover Phenomenon in Bulk Water, Confined Water and Protein Hydration Water. *J. Phys.: Condens. Matter* **2012**, *24*, 064103 (10pp).

(5) Debenedetti, P. G. Supercooled and Glassy Water. *J. Phys.: Condens. Matter* **2003**, *15*, R1669−R1726.

(6) Bonnaud, P. A.; Coasne, B.; Pellenq, R. J.-M. Molecular Simulation of Water Confined in Nanoporous Silica. *J. Phys.: Condens. Matter* **2010**, *22*, 284110 (15pp).

(7) Liu, E.; Dore, J. C.; Webber, J. B. W.; Khushalani, D.; Jähnert, S.; Findenegg, G. H.; Hansen, T. Neutron Diffraction and NMR Relaxation Studies of Structural Variation and Phase Transformations for Water/Ice in SBA-15 Silica: I. The Over-Filled Case. *J. Phys.: Condens. Matter* **2006**, *18*, 10009−10028.

(8) Demontis, P.; Gulín-González, J.; Jobic, H.; Masia, M.; Sale, R.; Suffritti, G. B. Dynamical Properties of Confined Water Nanoclusters: Simulation Study of Hydrated Zeolite NaA: Structural and Vibrational Properties. *ACS Nano* **2008**, *2* (8), 1603−1614.

(9) Hwang, D. W.; Chu, Ch.-Ch.; Sinha, A. K.; Hwang, L.-P. Dynamics of Supercooled Water in Various Mesopore Sizes. *J. Chem. Phys.* **2007**, *126*, 044702−7.

(10) Angell, C. A. Formation of Glasses from Liquids and Biopolymers. *Science* **1995**, *267*, 1924−1935.

(11) Ito, K.; Moynihan, C. T.; Angell, C. A. Thermodynamic Determination of Fragility in Liquids and a Fragile-to-Strong Liquid Transition in Water. *Nature* **1995**, *398*, 492−495.

(12) Mallamace, F.; Broccio, M.; Corsaro, C.; Faraone, A.; Wanderlingh, U.; Liu, L.; Mou, C.-Y.; Chen, S.-H. The Fragile-to-Strong Dynamic Crossover Transition in Confined Water: Nuclear Magnetic Resonanse Results. *J. Chem. Phys.* **2006**, *124*, 161102 (4pp).

(13) Faraone, A.; Liu, L.; Mou, C.-Y.; Yen, C.-W.; Chen, S.-H. Fragile-to-Strong Liquid Transition in Deeply Supercooled Confined Water. *J. Chem. Phys.* **2004**, *121* (No. 22), 10843−10846.

(14) Demontis, P.; Gulín-González, J.; Masia, M.; Suffritti, G. B. The Behaviour of Water Confined in Zeolites: Molecular Dynamics Simulations Versus Experiment. *J. Phys.: Condens. Matter* **2010**, *22*, 284106 (13pp).

(15) Suffritti, G. B.; Demontis, P.; Gulín-González, J.; Masia, M. Computer Simulations of Dynamic Crossover Phenomena in Nano-confined Water. *J. Phys.: Condens. Matter* **2012**, *24*, 064110 (11pp).

(16) Grünberg, B.; Emmler, Th.; Gedat, E.; Shenderovich, I.; Findenegg, G. H.; Limbach, H.-H.; Buntkowsky, G. Hydrogen Bonding of Water Confined in Mesoporous Silica MCM-41 and SBA-15 Studied by ^{1}H Solid-State NMR. *Chem.—Eur. J.* **2004**, *10*, 5689−5696.

(17) Long, Y.; Palmer, J. C.; Coasne, B.; Śliwińska-Bartkowiak, M.; Gubbins, K. E. Pressure Enhancement in Carbon Nanopores: A Major Confinement Effect. *Phys. Chem. Chem. Phys.* **2011**, *13*, 17163−17170.

(18) Jażdżewska, M.; Śliwińska-Bartkowiak, M. M.; Beskrovnyy, A. I.; Vasilovskiy, S. G.; Ting, S.-W.; Chan, K.-Y.; Huang, L.; Gubbins, K. E. Novel Ice Structures in Carbon Nanopores: Pressure Enhancement Effect of Confinement. *Phys. Chem. Chem. Phys.* **2011**, *13*, 9008−9013.

(19) Śliwińska-Bartkowiak, M.; Drozdowski, H.; Kempiński, M.; Jażdżewska, M.; Long, Y.; Palmer, J. C.; Gubbins, K. E. Structural Analysis of Water and Carbon Tetrachloride Adsorbed in Activated Carbon Fibres. *Phys. Chem. Chem. Phys.* **2012**, *14*, 7145−7153.

(20) Blicharski, J. S.; Gutsze, A.; Korzeniowska, A. M.; Lalowicz, Z. T.; Olejniczak, Z. Deuteron Spin-Lattice Relaxation Study of D_2 Secluded in the Supercages of Zeolite NaY. *Appl. Magn. Reson.* **2004**, *27*, 183−195.

(21) Birczyński, A.; Punkkinen, M.; Szymocha, A. M.; Lalowicz, Z. T. Translation and Reorientation of CD_4 Molecules in Nanoscale Cages of Zeolites as Studied by Deuteron Spin-Lattice Relaxation. *J. Chem. Phys.* **2007**, *127*, 204714−10.

(22) Lalowicz, Z. T.; Stoch, G.; Birczyński, A.; Punkkinen, M.; Ylinen, E. E.; Krzystyniak, M.; Góra-Marek, K.; Datka, J. Translational and Rotational Mobility of Methanol-d_4 Molecules in NaX and NaY Zeolite Cages: A Deuteron NMR Investigation. *Solid State Nucl. Magn. Reson.* **2012**, *45−46*, 66−74.

(23) Gedat, E.; Schreiber, A.; Albrecht, J.; Emmler, Th.; Shenderovich, I.; Findenegg, G. H.; Limbach, H.-H.; Buntkowsky, G. ^{2}H-Solid-State NMR of Benzene-d_6 Confined in Mesoporous Silica SBA-15. *J. Phys. Chem. B* **2002**, *106*, 1977−1984.

(24) Stepanov, A. G.; Alkaev, M. M.; Shubin, A. A. Molecular Dynamics of Iso-Butyl Alcohol Inside Zeolite H-ZSM-5 as Studied by Deuterium Solid-State NMR Spectroscopy. *J. Phys. Chem. B* **2000**, *104*, 7677−7685.

(25) Stepanov, A. G.; Alkaev, M. M.; Shubin, A. A.; Luzgin, M. V.; Shegai, T. O.; Jobic, H. Dynamics of Isobutane Inside Zeolite ZSM-5. A Study with Deuterium Solid-State NMR. *J. Phys. Chem. B* **2002**, *106*, 10114−10120.

(26) Abragam, A. *Principles of Nuclear Magnetism*; Oxford University Press: New York, 1961.

(27) Yasaka, Y.; Wakai, C.; Matubayasi, N.; Nakahara, M. Rotational Dynamics of Water and Benzene Controlled by Anion Field in Ionic Liquids: 1-Butyl-3-Methylimidazolium Chloride and Hexafluorophosphate. *J. Chem. Phys.* **2007**, *127*, 104506−8.

(28) Alam, T. M.; Dreyer, D. R.; Bielwaski, C. W.; Ruoff, R. S. Measuring Molecular Dynamics and Activation Energies for Quaternary Acyclic Ammonium and Cyclic Pyrrolidinium Ionic Liquids Using ^{14}N NMR Spectroscopy. *J. Phys. Chem. A* **2011**, *115*, 4307−4316.

(29) Yasaka, Y.; Klein, M. L.; Nakahara, M.; Matubayasi, N. Communication: Exploring the Reorientation of Benzene in an Ionic Liquid via Molecular Dynamics: Effect of Temperature and Solvent Effective Charge on the Slow Dynamics. *J. Chem. Phys.* **2011**, *134*, 191101−4.

(30) Yasaka, Y.; Klein, M. L.; Nakahara, M.; Matubayasi, N. Rotational Dynamics of Benzene and Water in an Ionic Liquid Explored via Molecular Dynamics Simulations and NMR T_1 Measurements. *J. Chem. Phys.* **2012**, *136*, 074508 (12pp).

(31) Lipari, G.; Szabo, A. Model-Free Approach to the Interpretation of Nuclear Magnetic Resonance Relaxation in Macromolecules. 1. Theory and Range of Validity. *J. Am. Chem. Soc.* **1982**, *104*, 4546−4559.
(32) Lipari, G.; Szabo, A. Model-Free Approach to the Interpretation of Nuclear Magnetic Resonance Relaxation in Macromolecules. 2. Analysis of Experimental Results. *J. Am. Chem. Soc.* **1982**, *104*, 4559−4570.
(33) Szymocha, A. M.; Birczyński, A.; Lalowicz, Z. T.; Stoch, G.; Krzystyniak, M.; Góra-Marek, K. Water Confinement in Faujasite Cages: A Deuteron NMR Investigation in a Wide Temperature Range. 1. Low Temperature Spectra. *J. Phys. Chem. A* **2014**, DOI: 10.1021/jp504648s.
(34) Woessner, D. E. Nuclear Magnetic Relaxation and Structure in Aqueous Heterogenous Systems. *Mol. Phys.* **1977**, *34*, 899−920.
(35) Peemoeller, H.; Stanley, J. A.; MacMillan, M. B.; Weglarz, W. P.; Bennett, J. C.; Corbett, J. M.; Hawton, M.; Holly, R. Hydration Study of Homopolypeptides by ^{2}H NMR. *Biopolymers* **2007**, *86*, 11−22.
(36) Slichter, C. P. *Principles of Magnetic Resonance*, 3rd ed.; Springer-Verlag: New York, 1990.
(37) Stoch, G.; Olejniczak, Z. Missing First Points and Phase Artifact Mutually Entangled in FT NMR Data − Noniterative Solution. *J. Magn. Reson.* **2005**, *173*, 140−152.
(38) Heuer, A.; Haeberlen, U. A New Method for Suppressing Baseline Distortions in FT NMR. *J. Magn. Reson.* **1989**, *85*, 79−94.